OPEN ACCESS
Journal of Multidisciplinary Applied Natural Science Vol. 5 No. 2 (2025) https://doi.org/10.47352/jmans.2774-3047.259
Check for updates
Research Article

Antiplasmodial and Metabolite Profiling of *Hyrtios* sp. Sponge Extract from Southeast Sulawesi Marine Using LC-HRMS, Molecular Docking, Pharmacokinetic, Drug-likeness, Toxicity, and Molecular Dynamics Simulation

Maria Ludya Pulung, Respati Tri Swasono, Eti Nurwening Sholikhah, Radite Yogaswara, Gian Primahana, Tri Joko Raharjo*

Received : December 9, 2024	Revised : February 17, 2025	Accepted : March 8, 2025	Online : May 23, 2025

Abstract
Hyrtios sponge is known to possess alkaloid compounds that may exhibit in vitro activity against *Plasmodium falciparum*. The aim of this study was therefore to isolate and characterise the antiplasmodial active compounds of *Hyrtios* sp. Sponges collected from the island of Podang-Podang, South Sulawesi, Indonesia. In addition, the LC-HRMS analysis was performed on the active fractions of methanol and ethyl acetate extract to evaluate their antiplasmodial activity. We also validated the in silico antiplasmodial activity of *Pf*DHFR-TS with molecular docking, pharmacokinetics, drug likeness, toxicity, and molecular dynamics analysis. The molecular docking studies showed that the synthesized extremes would have high binding affinity to *Pf*DHFR-TS, thus confirming their potential as powerful enzyme inhibitors. Moreover, the pharmacokinetic and drug-likeness calculations showed that all compounds met the requirements for sufficient resistance and bioavailability, indicating potential as therapeutic candidates. The results of the toxicity analysis indicated that the compounds had a relatively good safety profile, but some potential adverse reactions in the renal and cardiac vasculature could not be excluded. Molecular dynamics simulations confirmed that the complexes formed between the ligand and the target were stable, and the low RMSD value indicated that the active site interactions were also quite stable. These observations reinforce the notion that the extract from *Hyrtios* sp. not only shows remarkable antimalarial activity but also exhibits pharmacological properties of a prospective drug candidate, which encourages further work in the development of malaria combination therapy both in clinical assessment and comprehensive mechanism of action investigation.

Keywords: sponge, *Hyrtios* sp., antiplasmodial, *Pf*DHFR-TS, molecular docking

1. INTRODUCTION

Malaria is one of the deadliest diseases in the world and still continues to claim millions of lives [1]. According to WHO estimates, there were approximate 241 million cases of malaria and 627,000 deaths caused by the disease in the year 2020. The African region is the most malaria endemic region, accounting for approximately 95% of the cases and deaths [2]. Between the years 2010 and 2022, Papua Province in Indonesia recorded the highest number of malaria cases in the entire country [3]. The existence of numerous antimalarial medications is countered with the chronic threat of resistant Plasmodium strains which aids in the infection control [4]. There is increasing resistance among different types of *Plasmodium*, which makes the search for new antimalarial drugs urgent.

FCR3 *P. falciparum* is a model of therapeutic drug abuse, which in endemic areas may increase morbidity and mortality. Increasing reports of antimalarial medication resistance over the last ten years have highlighted the necessity of new, more potent medications to fight the illness. It is important to focus on using natural resources, like chemicals from the ocean, that show great potential as strong antimalarial treatments. Directing the challenge of resistance has two advantages: it expands the treatment options available and it fuels optimism about global malaria control [2][5]. Furthermore, the combination of some of these new medicines with older ones in a form of combination therapy appears to be effective in overcoming resistance [1].

Resistance to antimalarial drugs, such as chloroquine, emphasizes the need for new substances with unique mechanisms of action. Recent studies have indicated that bioactive compounds derived from natural sources, especially marine species like *Hyrtios* sponges, hold great promise as novel antimalarial agents. These

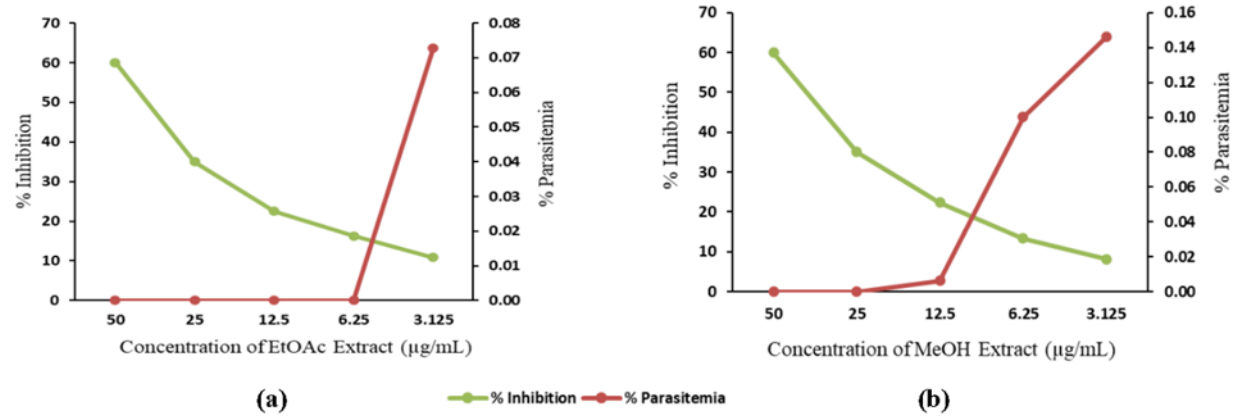

Figure 1. Percentage inhibition concentration versus parasitaemia of (a) EtOAc and (b) MeOH extracts.

compounds show antibacterial and anticancer properties and have the capacity to reduce malaria symptoms by means of several interactions with target enzymes in the *P. falciparum* parasite [1][5]. Previous studies have shown that secondary metabolites of marine fungi have antimalarial properties. Alkaloids and terpenes were shown to be effective against the malaria parasite [5][6]. The exploration of marine biological resources is therefore a calculated step towards developing new treatments in the face of the malaria resistance challenge.

The sponge *Hyrtios* cf. erecta extract dichloromethane (CH_2Cl_2), which was gathered from Fiji, contains two novel alkaloids (homofascaplysin and fascaplysin) that have been demonstrated to have strong in vitro activity against *P. falciparum* [7]. Reports indicate that *Hyrtios* sponge extract from Bali, Indonesia, may be effective against malaria, with IC_{50} values of 12.98 ± 1.88 and 19.81 ± 0.75 µg/mL for the *P. falciparum* 3D7 and FCR3 variants, respectively [8]. Pelorol from *Hyrtios erectus* found in Chuuk Island, Federated States of Micronesia, effectively inhibited *P. falciparum* with an IC_{50} value of 0.8 µM during scuba diving [9]. New specimens of *H. reticulatus* and *H. erectus* from Southwest Sulawesi, Indonesia have yielded several tryptamine-derived alkaloids, still their pharmacological activity has not been reported [10]. Isolation of Hyrtioreticuli A–E compounds from *Hyrtios* sponge taken from North Sulawesi Sea waters have been successfully carried out. In this research, samples of *Hyrtios* sponge (family Thorectidae) were collected from Podang-Podang Island, South Sulawesi, Indonesia. Studies on the chemical content of *Hyrtios* sponge from Podang-Podang Island have never been reported, thus this study aims to determine the antiplasmodial activity of crude methanol (MeOH) and ethyl acetate (EtOAc) extracts from the samples and identify their chemical composition using liquid chromatography-high resolution mass spectrometry (LC-HRMS) analysis. Furthermore, the hypothetical chemical structure obtained from LC-HRMS analysis was confirmed for its properties as a drug candidate using pharmacokinetic, drug-likeness, molecular docking and molecular dynamics simulation methods.

2. MATERIALS AND METHODS

2.1. Material and Extraction Process

The *Hyrtios* sp. sponge was hand collected on Poddang-Podang Island, off the coast of South Sulawesi, Indonesia, and stored at -25 °C before the chemical analysis. The identity was confirmed by the Natural Product Laboratory of Diponegoro University in Indonesia. We washed the samples to remove impurities and shrunk them to facilitate extraction. A mixture of MeOH/CH_2Cl_2 (1:1) was used to extract the frozen sponge materials (400 g wet weight) three times (3×200 mL) at room temperature. The organic extract was diluted under lower pressure and subsequently submerged in 100 mL of MeOH/H_2O (9:1) solution. To obtain 2.1 g of *n*-hexane residue, the mixture was extracted using *n*-hexane (3×100 mL). After diluting the remaining methanolic layer with H_2O to a 3:2 MeOH/H_2O ratio, the methanolic layer was extracted as MeOH

and EtOAc extracts (3×100 mL) alternately [11].

2.2. Instrumentation

The instruments used were rotary evaporator (Buchi), incubator oven (Memmert), LC-HRMS Thermo Exactive Orbitrap (Thermo Scientific), and UV-Vis spectrophotometer (Thermo Fisher Scientific G10S). Molecular docking used Yasara Structure software version 23.4.25 and Autodock 4.2.6 contained in AMDock software [12]. Yasara Structure was used to determine re-docking and docking poses, while Autodock was used to determine binding affinities and inhibition constants.

2.3. Culture of P. falciparum

The modified Trager and Jensen method was used to culture *P. falciparum* FCR3 for antiplasmodial activity test [13]. In human O red blood cells, *Plasmodium* was cultivated at a 3% haematocrit in RPMI 1640 medium containing 10% human O serum. Two grams of $NaHCO_3$, 10.43 g of RPMI 1640 powder, 6 g of HEPES, 25 mg of gentamycin, and 1 L of sterile distilled water were combined to create the media. The media was made to have a pH of ±7.2. It was kept cold, at 4 °C, after being sterilized with a 0.22 µm filter. To produce the whole Plasmodium culture media, human serum was added to the media at a concentration of 10%. Every 24 h, the Plasmodium cultures were monitored while incubating in a candle jar at 37 °C.

2.4. In Vitro Antiplasmodial Activity Assay

The addition of 5% D-sorbitol helped the *Plasmodium* reach the ring stage by synchronize it. *Plasmodium* was centrifuged at 1000 rpm for 10 min in a conical tube after being transferred from the culture flask. After supernatant removal, sterile 5% sorbitol was added and incubated at 37 °C for 10 min. After the second centrifugation, supernatant was removed and culture media was added to wash the *Plasmodium*. The supernatant was removed after subsequent centrifugation, leaving only the *Plasmodium* in the ring stage. Parasites were

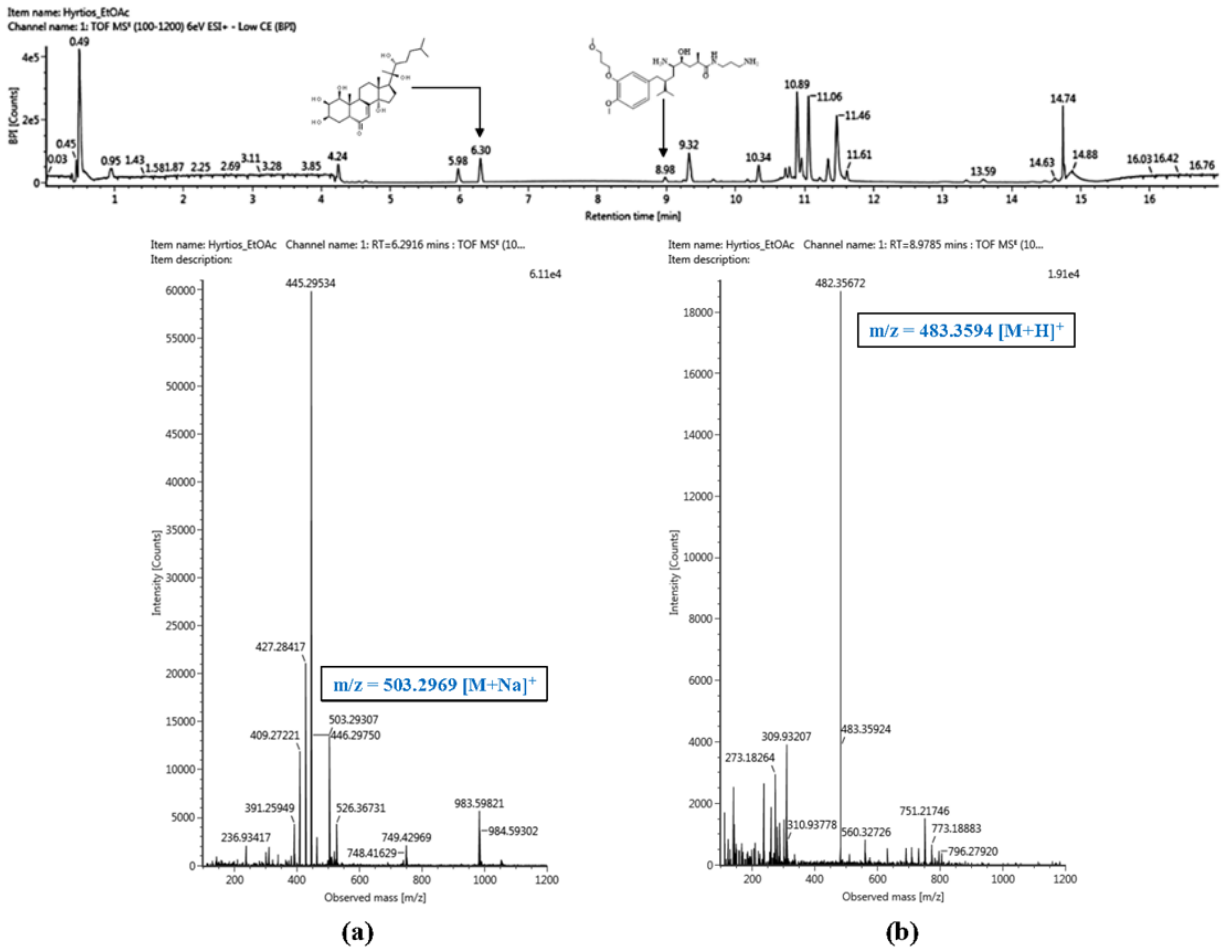

Figure 2. Mass spectrum of tentatively identified compounds off EtOAc extracts.

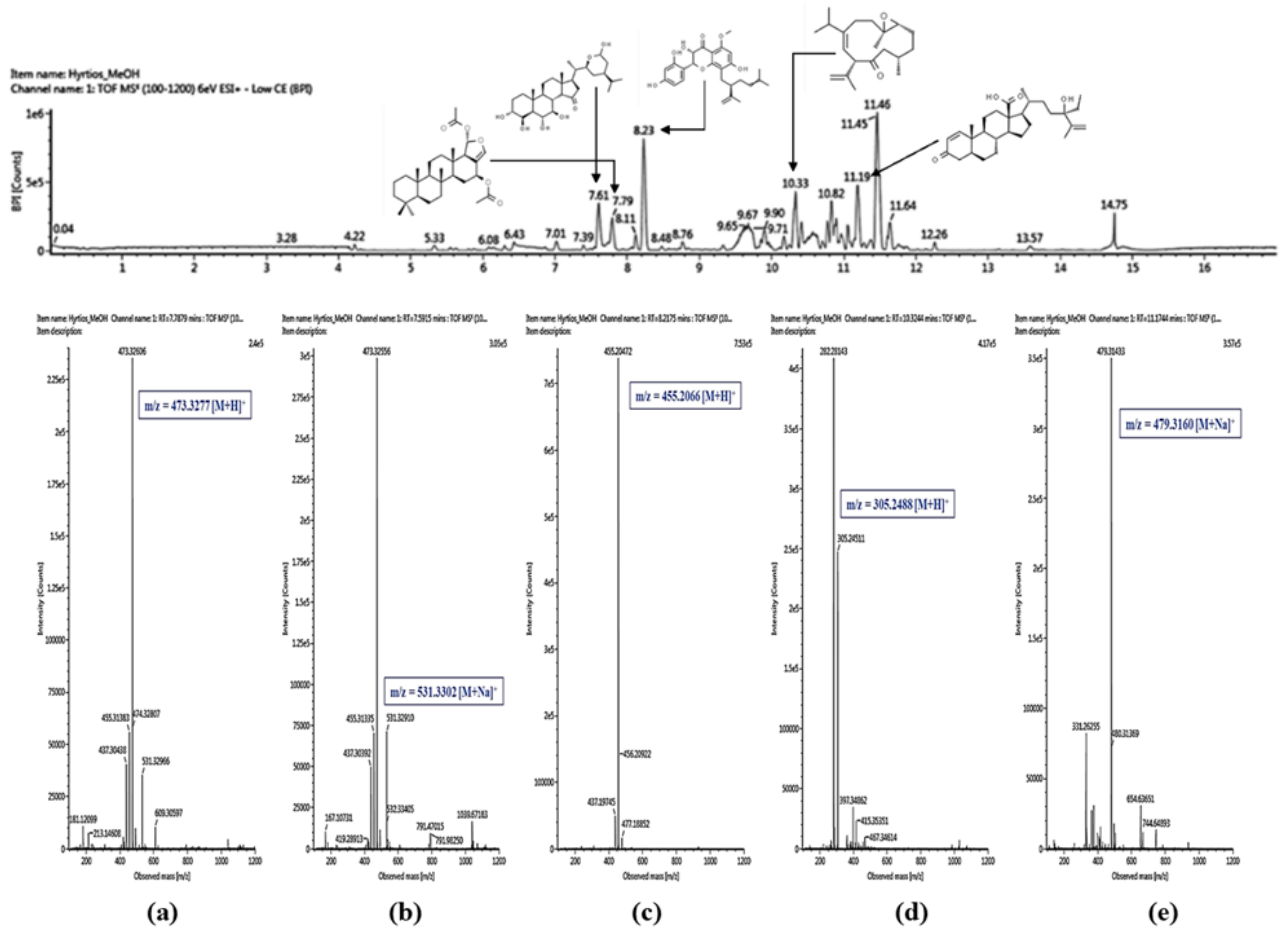

Figure 3. Mass spectrum of tentatively identified compounds of MeOH extracts.

detected by thin blood smear. The test used RPMI medium with 10% human O serum and 1% parasitaemia at 2% haematocrit.

In RPMI medium, dissolved compounds were tested. The test compounds (100 µL) were added to a 96 well microplates at various concentrations, followed by 100 µL of Plasmodium suspension. The concentration series was repeated three times and stored at 37 °C for 72 h. Thin blood smears stained with 10% Giemsa were examined at 1,000× magnification under a light microscope after incubation. At least 1,000 red blood cells in a thin blood smear were analysed for parasitaemia and *Plasmodium* growth inhibition. A 100% growing *Plasmodium* culture without compound testing was the control. Probit analysis determines the IC_{50} value, which is the compound concentration required to inhibit 50% of *Plasmodium* growth. Lower IC_{50} indicates stronger antiplasmodial activity. The IC_{50} value criteria for each extract followed the previous study [14].

2.5. Chemical Constituents Analysis Using LC-HRMS

The active sample was measured at 1 mg/mL, mixed with MeOH, sonicated for 10 min, and filtered through a 0.22 µm PTFE syringe filter. LC-HRMS analysis was performed using a Water XevoG2 XS Qtof. Separation was carried out using a Water BEH C18 column (2.1×50 mm, 1.7 µm) as the stationary phase. The mobile phases were acetonitrile (B) and MilliQ water (A) with 0.1% formic acid. Gradient elution took 17 min at 0.3 mL/min. The process started at 5% B, increased to 100% B in 10 min, maintained this concentration for 3 min, and then returned to the gradient for 3 min. The injection volume was 1 µL, and each run was compared with a blank sample. Analysis of isotopic abundance was conducted and the optimal empirical formula was presented. Database searches were performed with ChemSpider (https://legacy.chemspider.com/) and online chemical database (https://www.chemnetbase.com). The retrieved databases were examined for compounds

within the genera with LC-HRMS matched molecular formulas or masses. Experimental data were compared with the literature to identify any matches. Preliminary compound assignments were determined upon the identification of matches. Parameters for mass spectrometry analysis included 40 °C column temperature and 100–1,200 Da mass range. The capillary voltage was 2 kV and the cone voltage 30 V. The source and desolvation temperatures were 120 and 500 °C, respectively. We set the cone gas flow at 50 L/h and the desolvation gas flow at 1000 L/h. The collision energy was rose from 10 to 40 eV. Leucine enkephaline was administered every 10 s throughout the run to correct internal mass [15].

2.6. Molecular Docking Against Mutant PfDHFR-TS

Molecular docking studies were performed on *Hyrtios* compounds, i.e., zoanthusterone, pterosterone, inokosterone, and ajugasterone C in EtOAc extracts as well as hyrtiosin E, contignasterol, kushenol N, and deoxoscalarin acetate in MeOH extracts. These were evaluated against mutant *Pf*DHFR-TS with a Protein Database Bank (PDB) ID of 1J3J obtained from https://www.rcsb.org/structure/1J3J. The target protein was prepared using YASARA Structure (v. 23.5.19) software to separate the three-dimensional crystal structure and pyrimethamine as the native ligand. The molecular docking protocol used dock_run.mcr script of YASARA Structure. The receptor-ligand complex was re-docked 1000 times with 25 iterations to validate docking protocol, and the resulting ligand pose showed an root mean square deviation (RMSD) value of less than 2 Å (0.2734 Å), indicating a satisfactory confidence level [16][17]. The entire structure of *Hyrtios* compounds were selected from https:// www.chemspider.com/Default.aspx. The inhibition constant (K_i) value measures the half maximum inhibition of an enzyme by a chemical substance and is used to assess the impact of substrates and inhibitors on enzyme function and biological activity. Compounds having inhibition constants below 100 mM are considered potential inhibitors, while those above 100 mM are considered non potent inhibitors [18]-[20]. The molecular docking results analysis using PyMOL and Web Server Analyzer, namely Protein-Ligand Interaction Profiler (https://lip-tool.biotec.tu-dresden.de/plip-web/lip/index).

2.7. Pharmacokinetic, Druglikeness, and Toxicity Prediction

In silico pharmacokinetic and drug-likeness analysis predicts drug interactions, determines dosage, identifies side effects, and optimises drug candidates. Computational simulations, QSAR modelling, virtual screening, and other in silico methods allow researchers to filter potential chemicals based on biophysical and pharmacokinetic properties, reducing drug development costs and time. Furthermore, this study is crucial for ensuring the bioavailability of medications, which laboratory tests must confirm for greater accuracy. SwissADME web server http://www.swissadme.ch/ was used to conduct the pharmacokinetics and druglikeness analyses of small molecules. The following pharmacokinetic and druglikeness parameters are used: Lipinski, Ghose, Veber, Egan, Muegge, bioavailability score, synthetic accessibility, GI absorption, BBB permeant, P-gp substrate, CYP1A2 inhibitor, CYP2C19 inhibitor, CYP2C9 inhibitor, CYP2D6 inhibitor, CYP3A4 inhibitor, Log Kp (skin permeation) [21]-[23].

ProTox 3 toxicity analysis assesses the health risks from chemical exposure, drug development side effects and environmental pollutant toxicity. It also assists academic and industrial researchers in studying chemical structure and toxicity and ensures compliance with chemical safety requirements. In toxicology education, this tool helps understand compound risks and informs health, pharmaceutical, and environmental decisions. Prediction of toxicity of small molecules were performed on the ProTox 3.0 web server https://tox.charite.de/protox3/. The toxicity parameters used in evaluating small molecules are LD_{50} predicted, hepatotoxicity, neurotoxicity, nephrotoxicity, respiratory toxicity, and cardiotoxicity [24][25].

2.8. Molecular Dynamics Simulation

After molecular docking EtOAc and MeoH compounds, molecular dynamics simulations were run every 100 ns to determine the stability of the

Table 1. The EtOAc and the MeOH extract chemical structures of identified compounds.

Compounds ID	Name	Binding affinity (kcal/mol)	Inhibition constant K_i (μM)	Contact residues
EtOAc extract				
9246029	Zoanthusterone	-11.68	1.39	*Hydrophobic*: Leu40, Leu46, Phe58, Ile112, Ile164 *H-bond*: Ala16, Asn108, Ile164
25038605	2*R*,4*S*,5*S*,7*S*)-5-Amino-*N*-(3-aminopropyl)-4-hydroxy-7-[4-methoxy-3-(3-methoxypro-poxy) benzyl]-2,8-dimethylnon-anamide	-11.5	1.22	*Hydrophobic*: Leu46, Met55, Phe58, Ile112, Leu119 *H-bond*: Asn108, Ser111 *π-stacking*: Phe58
MeOH extract				
10355791	Calyculone A	-7.99	3.72	*Hydrophobic*: Ala16, Leu46, Phe58, Ile112, Ile164
20169597	Deoxoscalarin acetate	-8.07	2.74	*Hydrophobic*: Leu40, Leu46, Phe58, Pro113, Tyr170
10480828	Hyrtiosin E	-12.09	1.37	*Hydrophobic*: Ile14, Leu46, Phe58, Ile112, Pro113, Phe116 *H-bond*: Asn108
57257125	Kushenol N	-10.13	3.56	*Hydrophobic*: Leu40, Leu46, Phe58, Ile112, Ile164 *H-bond*: Ala16, Ser111
331982	Contignasterol	-11.63	1.15	*Hydrophobic*: Ala16, Leu46, Phe58, Ile112, Pro113 *H-bond*: Ile14, Cys15, Ala16, Asn108, Ile164
Native ligand				
CP6	Pyrimethamine	-7.81	1.88	*Hydrophobic*: Ile112, Pro113, Phe58, Ile164 *H-bond*: Ile14, Cys15, Tyr170, Thr185 *π-stacking*: Phe58 *Halogen*: Asn108 *Salt bridges*: Asp54

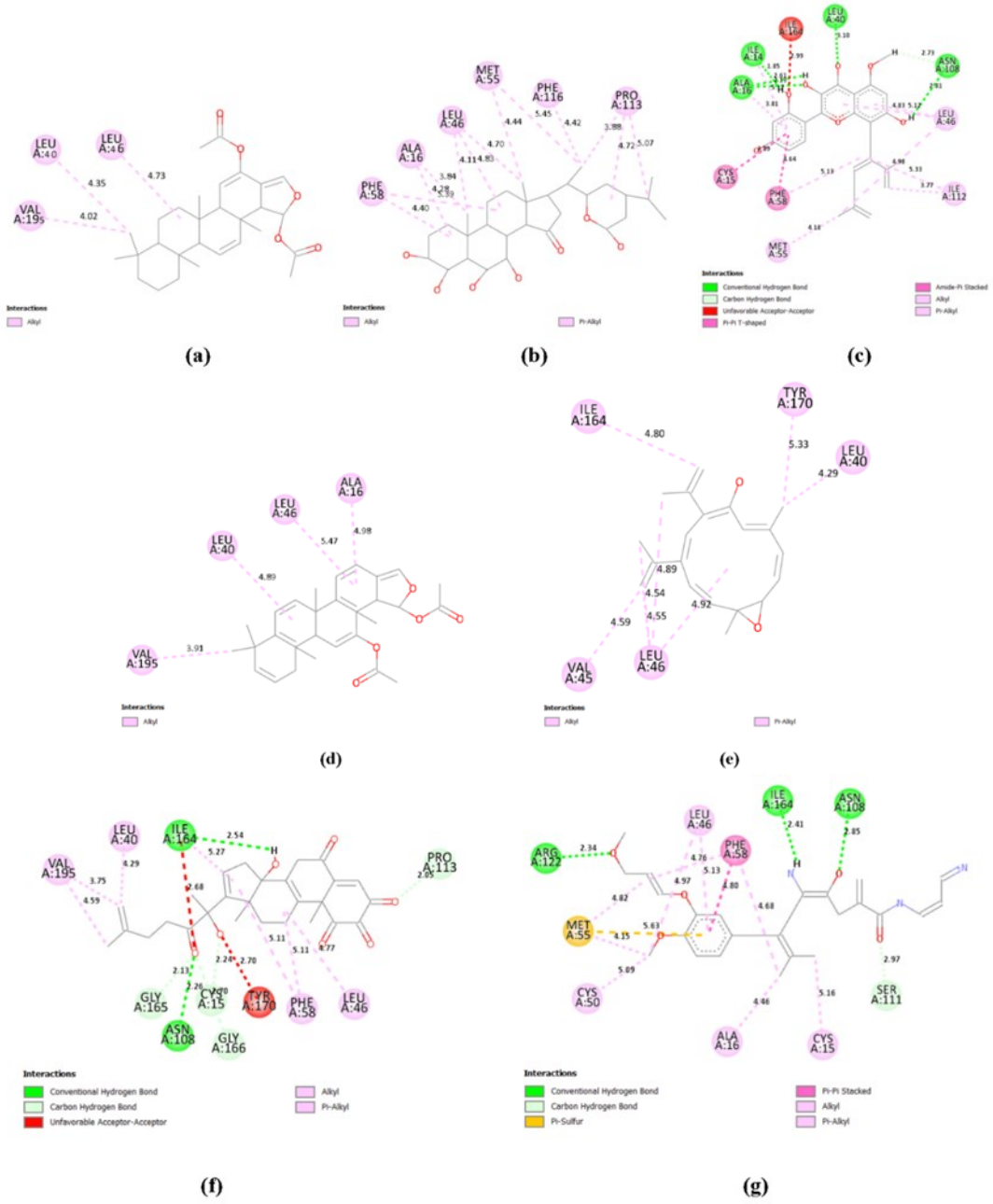

Figure 4. The non-covalent interactions of compounds (a) ID10480828, (b) ID331982, (c) ID57257125, (d) ID20169597, and (e) ID10355791 in the *Pf*DHFR-TS binding pocket of the MeOH extract; and compounds (f) ID9246029 and (g) ID25038605 in the *Pf*DHFR-TS binding pocket of the EtOAc extract, respectively.

complex formed between the extract ligand and the target binding pocket when H_2O molecules were added. Molecular dynamics simulations using YASARA STRUCTURE software with the AMBER14 force field and a simulation grid box was created with a radius of 10 A from the ligand to the target binding pocket area in the form of a cube. The system minimization energy used the steepest descent method, time step 2.5 fs, and simulation snapshots were stored at 100 ps intervals. Simulation analysis includes root mean square deviation (RMSD), radius of gyration (RoG), root mean square fluctuation (RMSF), changes in hydrogen bonds, solvent-accessible surface area (SASA), and binding energy (MMPBSA) [26].

3. RESULTS AND DISCUSSIONS

The Hyrtios sponge was macerated to break down its solid structure and extract its bioactive compounds. A 400-g sponge sample was collected and cleaned to remove dirt. To prepare for

extraction, the sample was frozen at -25 °C. The sponge was macerated in a 1:1 mixture of MeOH and CH_2Cl_2 solvents for three 200-mL soaks at room temperature. We chose this solvent because it effectively extracted both polar and non-polar compounds. The organic extract was concentrated under reduced pressure and absorbed into a 9:1 MeOH/H2O solution to obtain the extract fraction after maceration. This method stabilises bioactive compounds during extraction to maximize isolation. Low-pressure evaporation of EtOAc and MeOH extracts yields 1.05 and 3.94 g of more concentrated target compounds, respectively, as shown in Fig. S1.

3.1. Antiplasmodial Activity

Thorectidae includes *Hyrtios* reticulatus, a marine sponge. This organism produces many rare secondary metabolites, including macrolides, sesterterpenes, and alkaloids [27]. A number of these metabolites demonstrate significant biological activities [6]. We investigated the antiplasmodial activity of *Hyrtios* sponge through *in vitro* assay. This began with the evaluation of *P. falciparum* FCR3 strain towards the *Hyrtios* EtOAc and MeOH extracts. *Hyrtios* sponge extracts exhibited antiplasmodial activity with IC_{50} values of 1.31 ± 0.82 and 1.43 ± 0.32 µg/mL against FCR3, respectively. The extract samples showed decent activity characteristics. These findings indicated that the EtOAc and MeOH extracts from *Hyrtios* sp. potential for further research to find compounds that have antiplasmodial activity. In another study, antiplasmodial evaluation of the *Hyrtios reticulatus* EtOH extract from Bali, Indonesia showed moderate activity criteria against P. falciparum FCR3 variant, with an IC_{50} values at 41.90 ± 2.32 µg/ml [8]. That was not as strong as the inhibitory concentrations found in EtOAC and MeOH extracts of *Hyrtios* sp. from Podang-Podang Island. The results of *in vitro* antiplasmodial assay of EtOAc and MeOH extracts are shown in Table S1.

The impact of sample concentration variations on %parasitaemia and %inhibition is illustrated in Figure 1. The extract inhibited *P. falciparum* parasite growth more as the sample concentration increased. The higher the dose, the lower the level of parasitism or the percentage of total erythrocytes that are infected with P. falciparum. The EtOAc extract from the *Hyrtios* sponge blocked 77.04% of the activity at a concentration of 31.25 µg/mL, and this increased to 100% at a concentration of 62.5.

Additionally, EtOAc extract reduced parasitaemia levels from 31.25 µg/mL to 0% at concentrations of 62.5, 125, 250, and 500 µg/mL (Fig. 1(a)). In Fig. 1(b), the MeOH extract inhibition increased by 50.01% from 31.25 µg/mL to 70.78% and 98.97% at 62.5 and 125 µg/mL concentrations. The increase occurred at 100% concentrations of 250 and 500 µg/mL. As a result, parasitaemia levels decreased from 31.25 µg/mL to 1.00% and from 62.5 to 125 µg/mL by 0.06%. The parasitaemia level was 0% at 250 and 500 µg/mL concentrations. Active compounds in the *Hyrtios* sponge allow these extracts to inhibit the growth of the *P. falciparum* parasite.

3.2. Profiling of Compounds Using LC-HRMS Analysis

LC-HRMS results showed only 4 compounds appeared in the EtOAc extract and 2 of them presented viable chromatogram results, specifically, only a single signal appeared in the sample. In the EtOAc extract, there are 4 spectra from the analysis results, but the structure of 2 spectra is not identified, so further stages are needed to identify the compound structure of the 2 spectra. The 2 identified spectra include a peak at RT 6.31 minutes, identifying the presence of compound $C_{27}H_{44}O_7$, and were characterized by m/z 503.2969 (Fig. 2(a)). At retention time (RT) 8.98 min, compound $C_{26}H_{47}N_3O_5$ was identified and indicated by the fragment ion at m/z 483.3594 (Fig. 2(b)).

The relationship between intensity vs. observed mass (m/z) and retention time is crucial for LC-HRMS structure determination of new compounds. In spectrum (a), the dominant peak at m/z 503.2969 [M+Na]+ is intense and a major component, while fragmentation peaks reveal derivatives. The primary peak at m/z 483.3594 [M+H]+ in the spectra (b) is less intense, suggesting it may be less represented (Table S2). Compared to spectrum (a) (6.2916 min), spectrum (b) (8.9785 min) has stronger interaction with the stationary phase, suggesting greater polarity or complexity. Integrating intensity, observed mass, and retention time analyses helps researchers hypothesise the structures of new compounds in extracts, with fragmentation patterns

aiding structural elucidation.

LC-HRMS analysis of the MeOH extract showed that there are 5 compounds. Compound $C_{29}H_{44}O_5$ was identified at RT 7.79 min and characterized by the fragment ion at m/z 473.3277. The compound $C_{29}H_{48}O_7$ was characterized by the presence of fragment ion at m/z 531.3302, emerged at RT 7.61 min. Fragment ion at m/z 455.2066 indicated the presence of compound $C_{26}H_{30}O_7$ which emerged at RT 8.23 min. The peak at RT 10.32 min identified the presence of compound $C_{20}H_{32}O_2$, it is characterized by the fragment ion at m/z 305.2488. At the RT 11.19 min, compound $C_{29}H_{44}O_4$ was identified and indicated by the fragment ion at m/z 479.316 (Table S3).

We found varying insights for each spectrum from the MeOH extract. In Fig. 3(a) spectrum, with a retention time of 7.879 min, the dominant peak at m/z 473.3277 $[M+H]^+$ shows high intensity, indicating it may be a major component, while additional peaks suggest possible fragments aiding in structural analysis. Fig. 3(b) spectrum at 7.591 min reveals the main peak at m/z 531.3302 $[M+Na]^+$, indicating potential sodium binding, with sufficient intensity for further fragment analysis. Fig. 3(c) spectrum at 8.2175 min has a primary peak at m/z 455.2066 $[M+H]^+$, suggesting stronger interaction with the column, indicated by the longer retention time and additional peaks under 500 m/z for potential fragmentation insights. Fig. 3(d) spectrum shows the main peak at m/z 305.2488 $[M+H]^+$ with the highest intensity at 10.324 min, indicating high polarity and additional fragmentation peaks guidance. Finally, in Fig. 3(e) spectrum with a retention time of 11.174 min, the peak at m/z 479.3160 $[M+Na]^+$ supports the likelihood of complex structures due to the longest retention time. Overall, the analysis of how intensity indicates concentration, observed mass helps in determining molecular weight, and varying retention times reflect the compounds' interaction with the column provides a comprehensive framework in the identification and structural elucidation of new compounds within these extracts.

We performed several steps to verify these compounds' authenticity and uniqueness. First, ID9246029 and ID25038605 were confirmed as new compounds by extensive searches in several reliable databases. We got structural data and relevant information from the Dictionary of Marine Natural Products and ChemSpider web server. This search yielded no compounds with the same chemical structure, indicating they have not been previously reported in the scientific literature. Furthermore, additional verification was conducted using spectral data from LC-HRMS analysis. We obtained information regarding the molecular masses and fragmentation patterns of the separated compounds. This spectral data was compared with records in various scientific publications to ensure that there were no similarities with known compounds. This process of spectral analysis was a crucial step in supporting our claim that both compounds possess unique characteristics that distinguish them from other identified compounds.

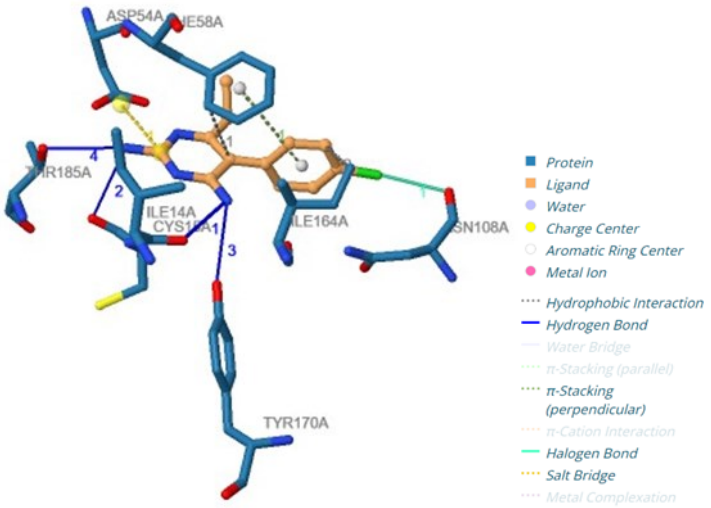

Figure 5. The non-covalent interactions of native ligand in 1J3J binding pocket.

This approach provides evidence for the distinctiveness of the extracted compounds. Since bioactive compounds from natural sources like marine sponges have shown remarkable therapeutic activities, these new compounds are important for drug development.

3.3. Molecular Docking Study

In this work, EtOAc and MeOH extracts of the identified chemical structures obtained from the ChemSpider web server are presented in Table S2 and Table S3. There are two compounds from the EtOAc extract (ID9246029 and ID25038605) and five compounds from the MeOH extract, i.e., ID10355791, ID20169597, ID10480828, ID57257125, and ID331982. The purpose of re-docking is to evaluate the validity of the docking processes. The native ligand (pyrimethamine) was docked into the active site of the double mutant *Pf*DHFR-TS receptor as part of the re-docking method. The initial conformation proved to be the most stable conformation, based on experimental data. Therefore, the conformation of the native ligand should not change significantly during this process.

The superimposed native ligand structures within the active site of *Pf*DHFR-TS are depicted in Fig. S2. The final conformation after re-docking is not significantly different from the initial conformation. The RMSD value of the re-docking process was obtained as 0.2734 Å. Due to its less than the 2.00 Å threshold, which is required for the re-docking procedure, this RMSD value is acceptable.

The binding affinity of CP6 was -7.81 kcal/mol. Molecular docking studies in this work showed high binding affinity values compared to CP6. ID10480828 had the highest binding affinity at -12.09 kcal/mol, followed by ID9246029, ID331982, ID25038605, ID57257125, ID20169597, and ID10355791 are -11.68 kcal/mol, -11.63 kcal/mol, -11.5 kcal/mol, -10.13 kcal/mol, -8.07 kcal/mol, and -7.99 kcal/mol, respectively.

The types of non-covalent interactions between critical amino acid residues and the native ligand (CP6) are listed in Table 1. CP6 interacts with Ile112, Pro113, Phe58, and Ile1642 residues through hydrophobic bonds, respectively. Other interactions are hydrogen bonds with Ile14, Cys15, Tyr170, and Thr185 residues; π-stacking with Phe58 residue; halogen bond with Asn108 residue; and salt bridges with Asp54 residue. These results are consistent with what was reported [28]. Non-covalent interactions resulted in a binding energy of -7.81 kcal/mol and a binding constant of 1.88 μM.

Inhibition constant (K_i) indicates the ability to inhibit the performance or interaction of enzyme on the substrate, where the smaller the K_i value, interactions between the ligand and the active side of receptor are maximized, and the stronger the bond formed. Compound ID331982 has the highest K_i value of 1.15 μM compared to other compounds in MeOH and EtOAc extracts. These values are also lower than CP6 (1.88 μM). In contrast, the lowest K_i value was found in compound ID10355791 with 3.72 μM. Two compounds from the EtOAc extract (ID25038605 at 1.22 μM and ID9246029 at 1.39 μM) and one from the MeOH extract (ID10480828 at 1.37 μM) have higher K_i values than CP6. Other compounds with lower K_i values than CP6 include ID20169597 (2.74 μM), ID57257125 (3.56 μM), and ID10355791 (3.72 μM).

The frequency distribution of common non-covalent interactions between proteins and ligands, covering hydrophobic, hydrogen, and π-stacking contacts. These interactions consist of weak hydrogen bonds, salt bridges, amide stacking, and cation-π interactions. More than 42,000 interactions include ligands containing aromatic rings, frequently serving as small molecule inhibitors. Aromatic rings are present in 76% of pharmaceuticals, with benzene being the most common type. Hydrophobic interactions predominantly engage side chains of leucine, valine, isoleucine, and alanine. Hydrophobic interactions facilitate the binding of drugs to receptors [29].

Additionally, the amino group and aromatic ring interaction (amide π-stacking) is essential for ligand binding. The interaction involves π-surface stacking of the amino bonds on the aromatic ring. The major amino acids involved in face-to-face amide π-stacking were glycine (19.4%) and tryptophan (17.9%). In edge-to-face geometry, glycine and leucine were the most frequently observed amino acids, with percentages of 20.1% and 13.0%, respectively [29].

However, the affinity, membrane permeability, and metabolic stability of compound are also

Table 2. Pharmacokinetic, drug-likeness, and toxicity prediction results.

Parameters	MeOH extract					EtOAc extract	
	ID331982	ID10355791	ID10480828	ID20169597	ID57257125	ID9246029	ID25038605
Pharmacokinetic							
GI absorption	High	High	High	High	High	High	High
BBB permeant	No	Yes	No	No	No	No	No
P-gp substrate	Yes	No	No	No	Yes	Yes	Yes
CYP1A2 inhibitor	No	No	No	No	No	No	No
CYP2C19 inhibitor	No	No	No	No	No	No	No
CYP2C9 inhibitor	No	No	Yes	Yes	No	No	No
CYP2D6 inhibitor	No	No	No	No	No	No	No
CYP3A4 inhibitor	No	No	No	No	Yes	No	No
Log K_p (skin permeation) cm/s	-7.30	-4.43	-4.16	-4.60	-5.52	-8.80	-8.48
Druglikeness							
Lipinski	Yes	Yes	Yes	Yes	Yes	Yes	Yes
Ghose	No	Yes	No	No	Yes	Yes	No
Veber	Yes	Yes	Yes	Yes	Yes	Yes	No
Egan	Yes	Yes	No	No	Yes	Yes	Yes
Muegge	Yes	No	No	No	Yes	Yes	No
Bioavailability Score	0.55	0.55	0.55	0.55	0.55	0.55	0.55
Synthetic accessibility	6.69	4.74	6.40	6.54	4.85	5.66	6.35
Oral Toxicity							
LD_{50} Predicted (mg/kg)	4000	20000	2000	590	2000	9000	4000
Toxic Class	5	6	4	4	4	6	5
Organ Toxicity							
Hepatotoxicity	Inactive	Inactive	Inactive	Inactive	Inactive	Inactive	Inactive
Neurotoxicity	Inactive	Inactive	Inactive	Inactive	Inactive	Inactive	Inactive
Nephrotoxicity	Active	Inactive	Inactive	Inactive	Active	Inactive	Active
Respiratory toxicity	Active	Inactive	Active	Active	Active	Active	Active
Cardiotoxicity	Active	Inactive	Active	Active	Inactive	Active	Inactive

enhanced by the specific interactions involving halo -gen atom, which is less frequent. A total of 351 CX --Y type interactions were identified, where X represents Cl, Br, or I, and Y denotes O, N, or S, originating from the protein side chain or backbone. The σ-holes (positive electrostatic potential) of the halogen atom (XB donor) and the nucleophile (XB acceptor) are the sites of these halogen bond (XB) interactions. Since fluorine is less polar and has higher electronegativity, it cannot form halogen bond interactions. Oxygen atom serves as the fore-most acceptor for halogen bonds, followed by sulfuric and nitrogen. Although asparagine, proline, arginine, and tryptophan residues are underrepresented, approximately 71% of halogen bonds are attached to the backbone of carbonyl oxygen atoms. The binding energy generated by the formation of salt bridges is insufficient to counteract the energy released by the dissolution of charged groups, which is why they make minimal contributions to protein stability. Salt bridges are contacts between positively charged nitrogen and negatively charged oxygen. Arginine amino acid residues exhibit a higher tendency to form salt bridges compared to lysine side chains due to their ability to generate cations during interactions [29].

Hydrophobic interactions are observed between compound ID10480828 with Ile14, Leu46, Phe58, Ile112, Pro113, and Phe116, as shown in Fig. 4(a). In addition, there is also a hydrogen bond with residue Asn108. Fig. 4(b) illustrates compound ID331982 hydrophobically interacting with Ala16, Leu46, Phe58, Ile112, and Pro113. Hydrogen bonds form with Ile14, Cys15, Tyr170, and Thr185 amino acid residues. Next, compound ID57257125 interacts hydrophobically with residues Leu40, Leu46, Phe58, Ile112, and Ile164 (Fig. 4(c)). The residues Ala16 and Ser111 form hydrogen bonds. Fig. 4(d) and Fig. 4(e) shows only hydrophobic interactions between amino acid residues Leu40, Leu46, Phe58, Pro113, and Tyr170 with compound ID20169597, as well as residues Ala16, Leu46, Phe58, Ile112, and Ile164 with compound ID10355791. Fig. 4(f) shows compound ID9246029 forming hydrogen bonds with residues Ala16, Asn108, and Ile164. Additional hydrophobic interactions occur with Leu40, Leu46, Phe58, Ile112, and Ile164. In contrast to compound ID25038605 in Fig. 4(g), Phe58 has π-stacking bonds, hydrophobic interactions with Leu46, Met55, Phe58, Ile112, and Leu119, and hydrogen bonds with Asn108 and Ser111.

The pose of compound ID331982 in the 1J3J binding pocket is the one that has the most hydrogen bonds, namely two strong hydrogen bonds on residues Ile14 and Ile164 with distances of 2.52 and 2.41 Å, respectively. Then three weak hydrogen bonds are at residues Cys15 (3.20 Å), Ala16 (3.46 Å), and Asn108 (3.16 Å). In addition, Ala16 is hydrophobically bound to the ligand, which increases the ligand's robustness at its active site. The amino acid residues that bind to ID331982 are similar to CP6 [28]. Residues Ile112, Pro113, and Phe58 form hydrophobic interactions with CP6 and ID331982. Residue Ile164 on CP6 is hydrophobic, while ID331982 is hydrogen bonded. Interestingly, residues Ala16, Asn108, and Ile164 are hydrogen bonds with compound ID331982, while Ile164 on CP6 is a hydrophobic interaction and Asn108 is a halogen bond as shown in Fig. 5. It is thought that this causes the binding affinity and inhibition constant values of ID331982 to increase by -3.82 kcal/mol and 0.73 µM compared to CP6.

Other best poses were followed by ID25038605, ID9246029, ID10480828, and ID57257125. ID25038605 has two important hydrogen bonds, Asn108 (3.11 Å) and Ser111 (2.45 Å), with one hydrophobically bound (3.65 Å) and π-stacked (4.07 Å on pi stacking type) residue, Phe58. ID9246029 has three important hydrogen bonds, namely Ala16 (2.34 Å), Asn108 (2.29 Å), and Ile164 (2.55 Å), where Ile164 (3.84 and 3.94 Å) also interacts hydrophobically. ID10480828 has one hydrogen bond with Asn108 (1.97 Å), and ID57257125 has two hydrogen bonds with Ala16 (2.59 and 2.98 Å) and Ser111 (2.53 Å).

3.4. Pharmacokinetic, Drug-likeness, and Toxicity Prediction

Table 2 shows the results of pharmacokinetic, drug-likeness, and toxicity predictions of the MeOH and EtOAc extract compounds.

The GI Absorption parameter indicates how well a compound can be absorbed when taken orally. High GI absorption suggests that the compound can effectively enter systemic circulation from the gastrointestinal tract. All MeOH and EtOAC compounds demonstrate high GI absorption The

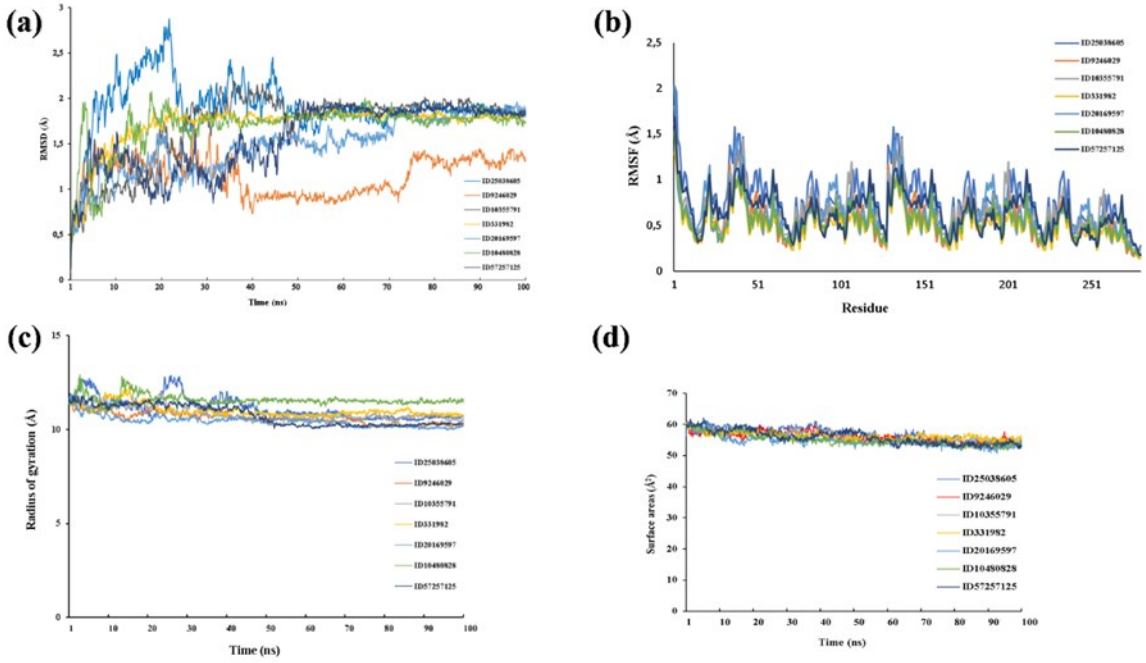

Figure 6. Molecular dynamics simulation analysis of (a) RMSD, (b) RMSF, (c) RoG and (d) SASA values of compounds ID10480828, ID331982, ID57257125, ID20169597 and ID10355791 for MeOH extract; and compounds ID9246029 and ID25038605 for EtOAc extract.

BBB permeability refers to the ability of the compound to cross the blood-Brain barrier, which is essential for neurotherapeutic medicinal products. All compounds in MeOH do not cross the BBB. Likewise, all compounds in EtOAc cannot penetrate the BBB. P-gp substrate indicates whether a compound can be recognised as a substrate by P-glycoprotein, an important transporter that facilitates drug exclusion from cells. Compounds ID10480828 and ID20169597 are P-gp substrates, while the others are not. Only ID9246029 functions as a P-gp substrate, whereas ID250384605 does not. CYP1A2 Inhibitor indicates whether a compound can inhibit the CYP1A2 enzyme, involved in drug and many endogenous compound metabolisms. Only ID20169597 is a CYP1A2 inhibitor, while the others are not. EtOAc compounds do not inhibit CYP1A2. A compound can inhibit the CYP2C19 enzyme, which affects drug metabolism. All compounds, MeOH and EtOAc, are not CYP2C19 inhibitors. Drug metabolism is linked to the CYP2C9 enzyme, which a compound's ability to inhibit is indicated by its CYP2C9 inhibitory properties. Only ID20169597 is a CYP2C9 inhibitor. The others are not in MeOH. Not all compounds inhibit EtOAc CYP2C9. An CYP2D6 inhibitor indicates a compound's ability to inhibit the enzyme that metabolises many drugs. Not all MeOH compounds are CYP2D6 inhibitors. ID250384605 inhibits CYP2D6, but ID9246029 does not. Many drugs depend on the CYP3A4 enzyme, which a compound can inhibit. Unlike the others, ID20169597 inhibits CYP3A4 in MeOH. ID9246029 does not inhibit CYP3A4, but ID250384605 does. Log K_p measures how quickly a compound penetrates the skin; higher values indicate better permeability. MeOH compounds have different permeabilities, as log K_p values range from -7.30 to -5.52. In contrast, EtOAc log K_p values range from -8.80 to -8.48, indicating lower skin permeability than methanol extract compounds.

Lipinski's rule predicts a compound's drug-likeness. No more than 5 hydrogen bond donors, 10 hydrogen bond acceptors, a molecular weight less than 500 Da, and an octanol-water partition coefficient (log P) less than 5 indicate orally active compounds. All compounds from both extracts met Lipinski's criteria with the category Yes. Ghose filter helps determine the drug-likeness of small molecules, indicating that they could be suitable for oral bioavailability if they meet certain criteria (e.g., molecular weight, log P, and number of rotational bonds). Compounds ID103557791, ID10480828,

and ID9246029 met these criteria. Veber's Rule states that a drug is most likely to be bioavailable if it has no more than 10 rotational bonds and is polar (described by a polar surface area less than 140 Å²). All MeOH compounds met Veber's criteria while one from the EtOAc extract did not, ID250384605. Egan rule suggests that compounds with a molecular weight below 500 Da and a log P of less than 5, along with fewer than 5 hydrogen bond donors, may exhibit good bioavailability. The compounds in MeOH showed good compliance, while one compound in EtOAc did not meet Egan's criteria. The Muegge Score evaluates the drug-likeness of a compound based on a variety of chemical properties, generally with values above 0 indicating potential drug-likeness. Most compounds met Muegge's criteria, indicating good drug-likeness. Bioavailability indicates the proportion of drug that enters the systemic circulation when introduced into the body and is available for action. All compounds showed comparable bioavailability. Synthetic accessibility evaluates how easily a compound can be synthesized. Higher scores indicate it is very difficult to synthesize. ID103557791 (4.74) and ID57257125 (4.85) showed ease of synthesis, while the other compounds showed moderate ease of synthesis.

The oral toxicity of MeOH shows a range of predicted LD_{50} values, indicating varying levels of toxicity. The highest LD_{50} (20,000 mg/kg) in ID103557791 indicates that this compound has low acute toxicity, is safe and non-toxic (class 6), while ID20169597 (590 mg/kg) is in class 4, which is harmful if swallowed. While EtOAc shows LD_{50} values indicating lower toxicity in ID9246029 (class 6) and ID250384605 (class 5), which are classified as non-toxic and may be harmful if swallowed. In organ toxicity, the MeOH extract showed greater concern with active nephrotoxicity, respiratory toxicity, and cardiotoxicity. This indicates potential adverse effects on the kidneys and respiratory system, as well as effects on the heart. While the EtOAc extract had a less concerning profile, with most organ toxicity parameters inactive, although it also showed active respiratory toxicity.

Both extracts showed favourable pharmacokinetic and drug-like properties as drug candidates. Attention should be paid to their toxicity profiles. Ethanol acetate appears harmless but may need further testing for toxicological effects, especially on the respiratory system, while methanol has a higher risk of toxicity that may limit its clinical use.

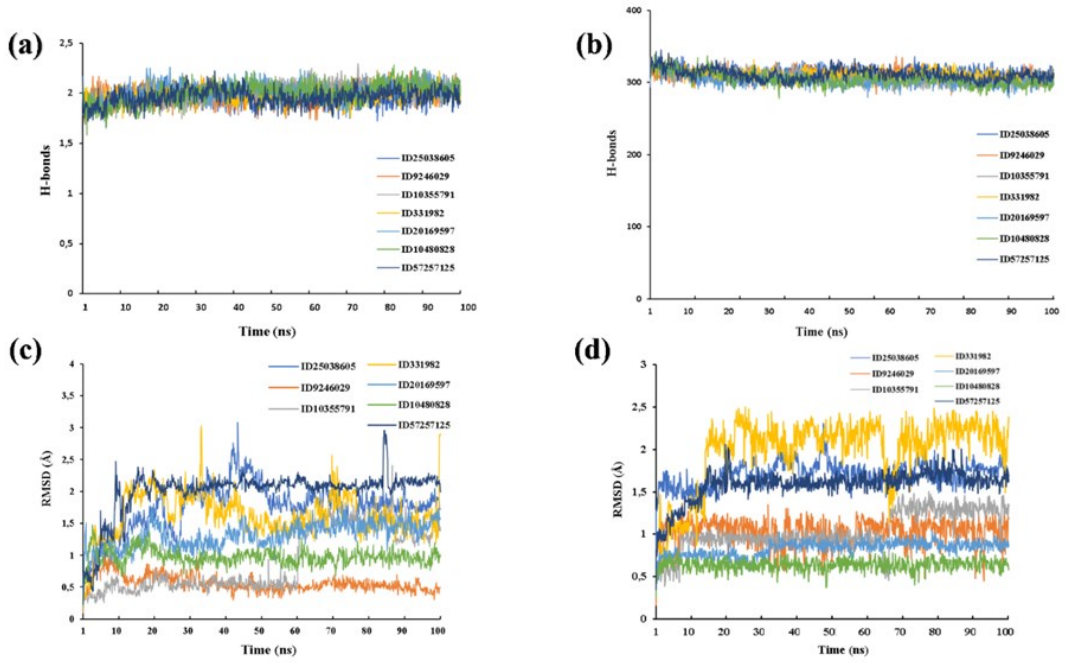

Figure 7. Relationship between the values of (a) changes in hydrogen bonds (H-bonds), (b) hydrogen bond interactions (solute-solvent), (c) RMSD ligand movement, and (d) RMSD ligand conformation in the binding pocket against simulation time (100 ns).

3.5. Molecular Dynamics Simulation

RMSD was used to measure structural changes per molecule during the simulation. A lower RMSD value indicates greater structural stability, while a higher value indicates greater fluctuations. Fig. 6(a) shows an analysis of the RMSD curve versus simulation time over 100 ns for seven compounds, it is evident that ID2503605 (blue) exhibits significant initial fluctuations before stabilising at around 2 Å, while ID9246029 (orange) shows a substantial increase in RMSD, particularly after 70 ns, indicating instability. In contrast, ID10355791 (black) and ID331982 (yellow) demonstrate good stability with limited fluctuations, similar to ID2016987 (light blue), which also remains consistent. ID10480828 (green) experiences initial fluctuations but stabilises thereafter, whereas ID57257125 (grey) shows a similar pattern with high stability. Overall, the majority of the compounds reach equilibrium within that timeframe, albeit with variations in rate and stability, providing important insights for further studies on the dynamic behaviour of these compounds. RMSF measures the average fluctuations of each residue in the protein structure.

Higher RMSF values indicate greater flexibility, while lower values point towards increased stability (Fig. 6(b)). Compound ID25038605 (blue) shows several peaks in RMSF, suggesting that certain residues are highly flexible. The fluctuations are evident across multiple regions, indicating variable stability among different residues. Similar to ID25038605, ID9246029 (orange) exhibits noticeable peaks, particularly at residues around 51 and 201, indicating flexibility in these specific regions. ID10355791 (black) has relatively lower RMSF values for most residues compared to the others, suggesting that it confers more stability to the binding pocket, with fewer regions showing high fluctuation. ID331982 (yellow) shows a moderate pattern of fluctuations, with certain residues nearing the fluctuations observed for ID25038605 and ID9246029 but generally displaying lower RMSF values. The RMSF profile of ID20169597 (light blue) exhibits fluctuations, particularly in the central region, indicating some flexibility but still remaining relatively stable in comparison to ID25038605 and ID9246029. Similar to ID10355791, ID10480828 (green) shows lower RMSF values across most residues, indicating good stability and minimal fluctuations. ID57257125 (grey) shows a fluctuation profile that closely resembles that of ID331982, with moderate peaks suggesting flexibility but generally lower than the first two compounds. Thus, compounds such as ID10355791 and ID10480828 demonstrate better stability, as indicated by lower RMSF values across most residues. Compounds ID25038605 and ID9246029 exhibit significant flexibility, particularly in certain residues, which may imply potential instability in the binding pocket. The remaining compounds, while showing some degree of fluctuation, fall in between, suggesting varying levels of structural stability and flexibility.

The protein size and compactness were measured using radius of gyration (RoG) (Fig. 6(c)). High RoG values indicate an expanded or disordered structure, while low values indicate a compact structure. ID25038605 (blue) exhibits initial fluctuations but maintains stability with a RoG around 11 Å after 60 ns, indicating conformation stability. Although there are initial fluctuations, the RoG of ID9246029 (orange) appears to stabilise, but at a slightly higher range compared to ID25038605, around 12 Å. The RoG for ID10355791 (black) ranges between 10-11 Å, indicating that it is relatively more compact than the others, with minimal fluctuations. ID331982 (yellow) fluctuates between RoG values of 10 and 12 Å with reasonably good stability, although the fluctuations are greater compared to ID10355791. ID20169597 (Light blue) shows stability with a RoG that remains around 12 Å, indicating that the structure remains relatively compact. ID10480828 (green) has a very stable RoG, consistently around 11 Å, demonstrating good compactness. The RoG profile for ID57257125 (grey) shows greater fluctuations but remains within 11 to 12 Å, indicating structural instability. Thus, ID25038605 and ID9246029 are stable but have slightly higher structures than ID10355791 and ID10480828, which are more compact. Others, like ID331982 and ID20169597, are intermediately stable with fluctuations. The RoG analysis reveals these compounds' conformation and structural stability over 100 ns.

SASA was used to measure the surface area accessible to solvent around a molecule as seen in

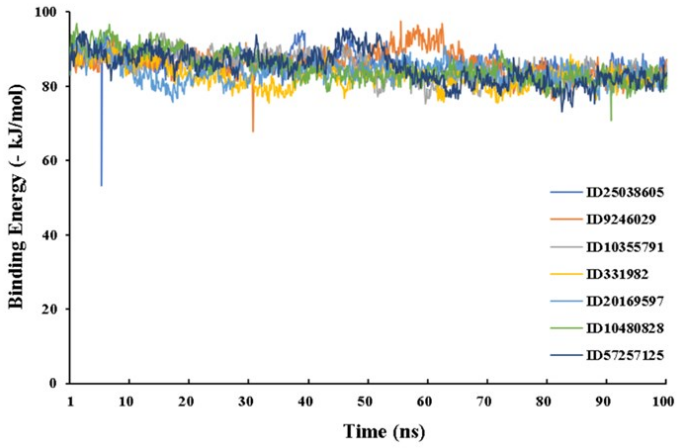

Figure 8. MM/PBSA binding energy values.

Fig. 6(d). Higher SASA values typically indicate that the protein's surface is more exposed, while lower values suggest a more compact structure. ID25038605 (blue) shows small but stable fluctuations, with a SASA ranging around 60 Å² throughout the simulation duration, indicating good compactness. The SASA of ID9246029 (red) is also stable and similar to that of ID25038605, remaining in a comparable range, suggesting that this structure is also quite compact. ID10355791 (grey) demonstrates a stable SASA around 55-60 Å², indicating good compactness with slightly lower variation. The SASA value of ID331982 (yellow) is slightly higher than the other compounds, ranging between 60–65 Å², indicating that this structure is somewhat more open than the others. ID20169597 (light blue) has consistent SASA values, also around 60 Å², reflecting good stability during the simulation period. ID10480828 (green) displays an SASA pattern like ID10355791, staying within 55-60 Å² and showing remarkable stability. ID57257125 (black) exhibits stable fluctuations, with SASA values slightly above 60 Å², denoting higher structural instability than other compounds.

Stability and conformation of proteins depend on H-bonds in Fig. 7(a). More H-bonds indicate stronger ligand-protein interactions. ID25038605 (blue) shows consistent fluctuations in H-bonds around 2 hydrogen bonds throughout the simulation, reflecting stable interactions with the target. The H-bonds for ID9246029 (orange) display a similar pattern, maintaining around 2 hydrogen bonds, indicating good stability in the interactions. ID10355791 (black) shows slight fluctuations with H-bond counts nearly the same, ranging from 1.5 to 2 bonds, suggesting that its interactions are also relatively stable. ID331982 (yellow) has slightly larger H-bond fluctuations but still maintains around 2 hydrogen bonds, indicating satisfactory stability. As ID331982, ID20169597 (light blue) fluctuates between 1.5 and 2.5 hydrogen bonds, indicating dynamic interactions. ID10480828 (green) has stable H-bonds around 1.5 –2 bonds, indicating good target interaction. ID57257125 (grey) fluctuates more than the others but remains within 1.5 to 2 hydrogen bonds, suggesting interaction instability. Hydrogen bond stability is high in most compounds, with values between 1.5 and 2.5. ID25038605 and ID9246029 have more stable interactions, while ID57257125 fluctuates more, indicating higher instability. Overall, the H-bond analysis shows the strength of ligand-protein interactions during the 100 ns simulation.

Protein stability and dynamics depend on the hydrogen bonds between ligands and solvents. Fig. 7(b) shows that more H-bonds indicate a stronger ligand-solvent interaction, which can affect binding efficiency and structural stability. ID25038605 (blue) shows stable fluctuations around 350 H-bonds, indicating regular solvent interactions during simulation. Similar to ID9246029 (orange), its H-bonds range from 300 to 400, indicating solvent stability. ID10355791 (black) shows a similar pattern, with H-bonds remaining stable around 300–350, demonstrating solid interactions with the solvent. ID331982 (yellow) has lower fluctuations with H-bonds mostly below 300, suggesting that binding with the solvent may be slightly less stable. The H-bonds for ID20169597 (light blue) range

from 300 to 370 with moderate fluctuations, indicating fairly good interactions with the solvent. ID10480828 (green) displays more stable H-bonds, remaining around 320–340, which indicates good interactions with the solvent. ID57257125 (grey) shows greater fluctuations but remains within the range of 300–400 H-bonds, indicating dynamic interactions with the solvent.

According to Fig. 7(c), lower RMSD values indicate that the ligand is stable and tightly bound, while higher values indicate pocket movement or flexibility. ID25038605 (blue) has the highest RMSD values (2.5-3.5 Å), indicating significant ligand movement in the binding pocket during simulation. The significant fluctuations suggest less stability. ID9246029 (orange) also shows notable RMSD fluctuations, with values hovering around 2 to 3 Å, indicating that it experiences some movement but remains somewhat more stable than ID25038605. ID10355791 (black) has a more stable RMSD profile, with values typically around 1.5 to 2 Å. The fluctuations are less pronounced, suggesting that the ligand maintains a better fit in the binding pocket. ID331982 (yellow) shows similar stability to ID10355791 with RMSD values around 1.5 to 2 Å but exhibits slightly more variation over the 100 ns, indicating some degree of movement. ID20169597 (light blue) also demonstrates a relatively stable RMSD profile, oscillating between 1 to 2 Å. It suggests that the ligand remains mostly bound within the pocket. The RMSD values for ID10480828 (Green) are consistently low, typically around 1 Å, indicating minimal movement within the binding site. ID57257125 (grey) has a similar RMSD profile to ID10480828, with values mostly below 1.5 Å, indicating ligand stability with minor fluctuations.

Fig. 7(d) displays the RMSD of the ligand atoms over time, measured after superposing on the reference structure of the ligand. ID25038605 (blue) shows a high RMSD fluctuation pattern, with values reaching nearly 2.5 Å. There is a significant increase in RMSD from 20 ns to 50 ns, before stabilizing with moderate fluctuations above 2 Å. ID331982 (yellow) has the highest RMSD value among the other compounds, often exceeding 2 Å. The conformation of this ligand appears to be very unstable, with large fluctuations throughout the simulation. The RMSD value of ID9246029 (orange) tends to be lower than ID25038605 and ID331982, stable around 1–1.5 Å. Although it has some fluctuations, it remains in a narrower range. ID10355791 (grey) is similar to ID9246029, but with slightly higher fluctuations and sometimes reaching around 1.5 Å. Stability is quite good, although there are some visible spikes. ID20169597 (green) shows good stability throughout the simulation, with very limited fluctuations. ID10480828 (red) shows a stable RMSD pattern but with a slightly higher value than ID20169597, around 1 Å. This compound has limited fluctuations and good stability. ID57257125 (light green) Similar to ID20169597, it is stable in the range of 0.5–1 Å. It shows minimal fluctuation, indicating a stable conformation. The simulations show that ID331982 and ID25038605 undergo major conformational changes due to their high RMSD values and instability. While ID20169597 and ID57257125 have lower RMSD, they are more stable and maintain consistent conformations. ID9246029 and ID10355791 are moderately stable, while ID10480828 is stable but more volatile than the two lowest RMSD ligands.

The AMBER14 force field MM/PBSA binding energy curves are shown in Fig. 8. The binding energy of ID25038605 (blue) fluctuates between 60 and 100 kJ/mol. Despite these spikes, its binding energy still indicates relative stability. ID9246029 (orange) has a binding energy that tends to be slightly higher than that of ID25038605, with a varying range but still below 100 kJ/mol. Its stability is quite good, with minimal fluctuations. ID10355791 (grey) exhibits a similar binding energy to ID9246029, with some spikes. The values vary within the same range but are not as volatile as those of ID25038605. ID331982 (yellow) has a more variable binding energy, sometimes reaching almost 100 kJ/mol but more often staying below 80 kJ/mol. This indicates that this compound is more unstable compared to the others. ID20169597 (green) displays stable binding energy, with repeated decreases below 80 kJ/mol. This good stability suggests that this ligand can bind to the target efficiently. ID10480828 (red) has a binding energy range that is relatively similar to ID20169597, but it often falls within a slightly higher range. This indicates consistent stability and minimal fluctuations, signifying good interaction

strength. The binding energy of ID57257125 (light green) fluctuates between 70 and 90 kJ/mol, indicating intermediate stability and a favourable interaction, but not as strong as ID20169597 or ID10480828. ID20169597 and ID10480828 have stable, low binding energies, indicating excellent binding efficiency, while ID331982 has a higher value, indicating instability. Higher fluctuations in ID25038605, ID9246029, and ID10355791 indicate weaker interactions. Although less instable than the two lowest compounds, ID57257125 is intermediately stable.

Fig. 9 shows the hydrogen bonds and hydrophobic interactions between important amino acid residues and the compounds from MeOH and EtOAc extracts in the *Pf*DHFR-TS binding pocket after 100 ns of molecular dynamics simulation. Compound ID10480828 forms hydrogen bonds with Asn108A. Hydrophobic interactions with other residues such as Leu46, Met55, Ile112, and Pro113 stabilise the binding pocket due to its large structure. The amino acids Ile14 and Ile164 hydrogen bond strongly with ID331982. Other interactions that also have the potential to stabilize the complex include Ala16, Met55, Phe58, and Pro113, respectively. Compound ID57257125 has two hydrogen bonds with residues Leu40 and Tyr170, as well as stacked and hydrophobic π-π interactions involving residues Phe58 and Leu46. In compound ID20169597, hydrogen bonds are formed with residue Asn51, while residues Leu46 and Phe58 exhibit hydrophobic interactions.

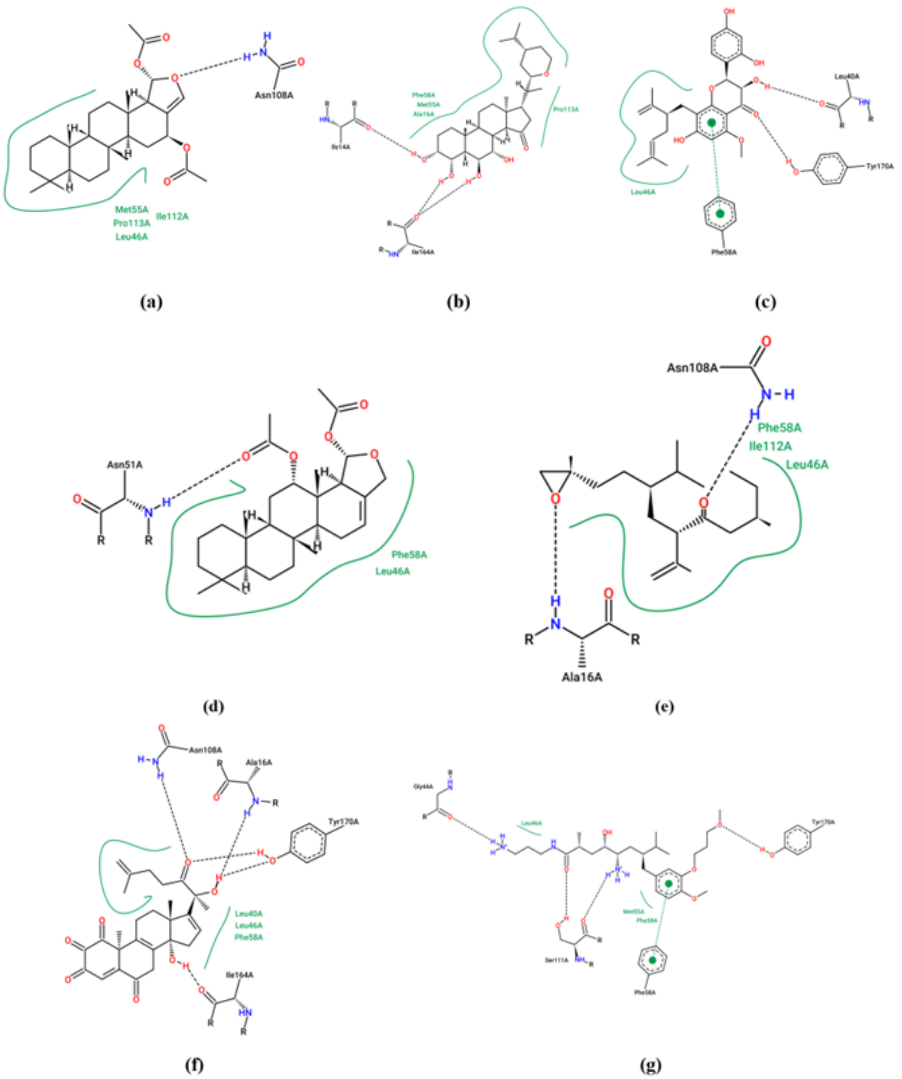

Figure 9. Interactions of compounds (a) ID10480828, (b) ID331982, (c) ID57257125, (d) ID20169597 and (e) ID10355791 for MeOH extract; and compounds (f) ID9246029 and (g) ID25038605 for EtOAc extract in the binding pocket of *Pf*DHFR mutant with a simulation time of 100 ns.

Compound ID10355791 shows two hydrogen bonds with residues Ala16 and Asn108, while hydrophobic interactions are present with residues Leu46, Phe58, and Ile112. Compound ID9246029 is quite stable, forming five hydrogen bonds, including one from Ala16, Asn108, Ile164, and two from Tyr170. Three hydrophobic interactions also support the stability of the complex, namely with Leu40, Leu46, and Phe58. Compound ID25038605 forms four hydrogen bonds, including one bond from Gly44 and Tyr170, and two bonds from Ser111. There is also one stacked π-π bond with residue Phe58 and three hydrophobic interactions with Leu46, Met55, and Phe58.

4. CONCLUSIONS

The study indicated that the *Hyrtios* sp. sponge extract had significant antiplasmodial activity, with the IC_{50} values for EtOAc and MeOH extracts being 1.31±0.82 µg/mL and 1.43±0.32 µg/mL, respectively. Molecular docking revealed that the extracted compounds attach well to the *Pf*DHFR-TS enzyme, indicating they could be effective inhibitors. Pharmacokinetic and drug-likeness analysis indicated that all compounds had good resistance and bioavailability, thus serving as potential therapeutic agents. Although some compounds showed kidney and heart side effects, toxicity analysis showed a relatively favourable safety profile. Molecular dynamics simulations supported the stability of the ligand-protein complex, and the low RMSD suggested that the compound is relatively stable in its binding to the active site. These results demonstrate that the *Hyrtios* sp. extract has promising antimalarial activity and fulfils drug candidate criteria, paving the way for clinical evaluation and mechanism-of-action studies of malaria combination therapy.

AUTHOR INFORMATION

Corresponding Author

Tri Joko Raharjo — Department of Chemistry, Universitas Gadjah Mada, Yogyakarta-55281 (Indonesia);
orcid.org/0000-0003-0615-5241
Email: trijr_mipa@ugm.ac.id

Authors

Maria Ludya Pulung — Department of Chemistry, Universitas Gadjah Mada, Yogyakarta-55281 (Indonesia); Department of Chemistry, Universitas Papua, Manokwari-98312 (Indonesia);
orcid.org/0000-0002-2458-7198

Respati Tri Swasono — Department of Chemistry, Universitas Gadjah Mada, Yogyakarta-55281 (Indonesia);
orcid.org/0000-0003-0762-6930

Eti Nurwening Sholikhah — Department of Pharmacology and Therapy, Universitas Gadjah Mada, Yogyakarta-55281 (Indonesia);
orcid.org/0000-0002-6545-8691

Radite Yogaswara — Department of Chemistry, Universitas Gadjah Mada, Yogyakarta-55281 (Indonesia); Department of Chemistry, Universitas Papua, Manokwari-98312 (Indonesia);
orcid.org/0000-0002-5937-6200

Gian Primahana — Research Centre for Pharmaceutical Ingredients and Traditional Medicine, National Research and Innovation Agency (BRIN), Banten-15314 (Indonesia);
orcid.org/0000-0001-8176-3859

Author Contributions

The authors have made significant contributions to their respective fields including Conceptualization, M. L. P. and T. J. R.; Methodology, M. L. P. and R. T. S.; Software, R. Y.; Validation, T. J. R., R. T. S. and E. N. S.; Formal Analysis and Data Curation, M. L. P. and G. P.; Investigation, M. L. P. and E. N. S.; Resources, Draft Preparation, Writing – Original and Writing – Review & Editing, M. L. P.; Visualization, R. Y. and G. P.; Supervision, T. J. R., R. T. S. and E. N. S.

Conflicts of Interest

The authors declare no conflict of interest.

SUPPORTING INFORMATION

Supplementary data associated with this article can be found in the online version at doi: doi.org/10.47352/jmans.2774-3047.259

ACKNOWLEDGEMENT

The authors express gratitude for the support of the Rekognisi Tugas Akhir (RTA) program at Gadjah Mada University with a reference number 5286/UN1.P1/PT.01.03/2024, and the first author would like to thank Indonesia Endowment Fund for Education Agency (LPDP), Ministry of Finance, and Republic of Indonesia for the support of the doctoral program scholarship at Gadjah Mada University (2022–2026).

REFERENCES

[1] M. Mushtaque and Shahjahan. (2015). "Reemergence of chloroquine (CQ) analogs as multi-targeting antimalarial agents: a review". *European Journal of Medicinal Chemistry.* **90** : 280-95. 10.1016/j.ejmech.2014.11.022.

[2] A. Monroe, N. A. Williams, S. Ogoma, C. Karema, and F. Okumu. (2022). "Reflections on the 2021 World Malaria Report and the future of malaria control". *Malaria Journal.* **21** (1): 154. 10.1186/s12936-022-04178-7.

[3] I. Fadilah, B. A. Djaafara, K. D. Lestari, S. B. Fajariyani, E. Sunandar, B. G. Makamur, B. Wopari, S. Mabui, L. L. Ekawati, R. Sagara, R. N. Lina, G. Argana, D. E. Ginting, M. E. Sumiwi, F. J. Laihad, I. Mueller, J. McVernon, J. K. Baird, H. Surendra, and I. R. F. Elyazar. (2022). "Quantifying spatial heterogeneity of malaria in the endemic Papua region of Indonesia: Analysis of epidemiological surveillance data". *The Lancet Regional Health – Southeast Asia.* **5** : 100051. 10.1016/j.lansea.2022.100051.

[4] J. C. Craft. (2008). "Challenges facing drug development for malaria". *Current Opinion in Microbiology.* **11** (5): 428-33. 10.1016/j.mib.2008.09.003.

[5] A. C. C. Aguiar, J. R. Parisi, R. N. Granito, L. R. F. de Sousa, A. C. M. Renno, and M. L. Gazarini. (2021). "Metabolites from Marine Sponges and Their Potential to Treat Malarial Protozoan Parasites Infection: A Systematic Review". *Marine Drugs.* **19** (3). 10.3390/md19030134.

[6] N. H. Shady, E. M. El-Hossary, M. A. Fouad, T. A. M. Gulder, M. S. Kamel, and U. R. Abdelmohsen. (2017). "Bioactive Natural Products of Marine Sponges from the Genus Hyrtios". *Molecules.* **22** (5). 10.3390/molecules22050781.

[7] G. Kirsch, G. M. Kong, A. D. Wright, and R. Kaminsky. (2000). "A new bioactive sesterterpene and antiplasmodial alkaloids from the marine sponge hyrtios cf. erecta". *Journal of Natural Products.* **63** (6): 825-9. 10.1021/np990555b.

[8] M. Mahfur, I. Purwantini, S. Wahyuono, and E. P. Setyowati. (2022). "In vitro antiplasmodial activities of the fractions of Hyrtios reticulatus sponge extract". *Journal of Applied Pharmaceutical Science.* 10.7324/japs.2022.120913.

[9] E. Ju, A. Latif, C. S. Kong, Y. Seo, Y. J. Lee, S. R. Dalal, M. B. Cassera, and D. G. I. Kingston. (2018). "Antimalarial activity of the isolates from the marine sponge Hyrtios erectus against the chloroquine-resistant Dd2 strain of Plasmodium falciparum". *Zeitschrift für Naturforschung C : Journal of Biosciences.* **73** (9-10): 397-400. 10.1515/znc-2018-0025.

[10] M. Salmoun, C. Devijver, D. Daloze, J. C. Braekman, and R. W. van Soest. (2002). "5-hydroxytryptamine-derived alkaloids from two marine sponges of the genus Hyrtios". *Journal of Natural Products.* **65** (8): 1173-6. 10.1021/np020009+.

[11] D. T. Youssef. (2005). "Hyrtioerectines A-C, cytotoxic alkaloids from the red sea sponge hyrtioserectus". *Journal of Natural Products.* **68** (9): 1416-9. 10.1021/np050142c.

[12] M. S. Valdes-Tresanco, M. E. Valdes-Tresanco, P. A. Valiente, and E. Moreno. (2020). "AMDock: a versatile graphical tool for assisting molecular docking with Autodock Vina and Autodock4". *Biology Direct.* **15** (1): 12. 10.1186/s13062-020-00267-2.

[13] W. Trager and J. B. Jensen. (2005). "Human Malaria Parasites in Continuous Culture". *Journal of Parasitology.* **91** (3): 484-486. 10.1645/0022-3395(2005)091[0484:Hmpicc]2.0.Co;2.

[14] O. Taglialatela-Scafati, E. Fattorusso, A. Romano, F. Scala, V. Barone, P. Cimino, E. Stendardo, B. Catalanotti, M. Persico, and C. Fattorusso. (2010). "Insight into the mechanism of action of plakortins, simple 1,2 -dioxane antimalarials". *Organic & Biomolecular Chemistry.* **8** (4): 846-56. 10.1039/b918600j.

[15] G. F. Swandiny, G. Primahana, M. E. Prastya, N. Ariani, D. Susanti, M. Hanafi, and S. Abdillah. (2023). "An ethnopharmacology study of Indonesian medicinal plants in Gunung Sari village as dipeptidyl peptidase-IV inhibitor". *Pharmacia.* **70** (2): 365-373. 10.3897/pharmacia.70.e104437.

[16] R. Yogaswara, M. L. Pulung, S. H. Yuliani, and E. P. Istyastono. (2020). "Docking-Guided 3D-QSAR Studies of 4-Aminoquinoline-1,3,5-triazines as Inhibitors for Plasmodium falciparum Dihydrofolate Reductase". *Indonesian Journal of Chemistry.* **20** (6). 10.22146/ijc.50674.

[17] G. Nugraha and E. P. Istyastono. (2021). "Virtual Target Construction for Structure-Based Screening in the Discovery of Histamine H2 Receptor Ligands". *International Journal of Applied Pharmaceutics.* 239-241. 10.22159/ijap.2021v13i3.41202.

[18] E. M. Terefe and A. Ghosh. (2022). "Molecular Docking, Validation, Dynamics Simulations, and Pharmacokinetic Prediction of Phytochemicals Isolated From Croton dichogamus Against the HIV-1 Reverse Transcriptase". *Bioinformatics and Biology Insights.* **16** : 11779322221125605. 10.1177/11779322221125605.

[19] F. Azimi, H. Azizian, M. Najafi, F. Hassanzadeh, H. Sadeghi-Aliabadi, J. B. Ghasemi, M. Ali Faramarzi, S. Mojtabavi, B. Larijani, L. Saghaei, and M. Mahdavi. (2021). "Design and synthesis of novel quinazolinone-pyrazole derivatives as potential alpha-glucosidase inhibitors: Structure-activity relationship, molecular modeling and kinetic study". *Bioorganic Chemistry.* **114** : 105127. 10.1016/j.bioorg.2021.105127.

[20] N. D. Zaharuddin, I. Barkia, W. Z. Wan Ibadullah, M. Zarei, and N. Saari. (2022). "Identification, molecular docking, and kinetic studies of six novel angiotensin-I-converting enzyme (ACE) inhibitory peptides derived from Kenaf (Hibiscus cannabinus L.) seed". *International Journal of Biological Macromolecules.* **220** : 1512-1522. 10.1016/j.ijbiomac.2022.09.142.

[21] A. Daina, O. Michielin, and V. Zoete. (2017). "SwissADME: a free web tool to evaluate pharmacokinetics, drug-likeness and medicinal chemistry friendliness of small molecules". *Scientific Reports.* **7** : 42717. 10.1038/srep42717.

[22] B. Bakchi, A. D. Krishna, E. Sreecharan, V. B. J. Ganesh, M. Niharika, S. Maharshi, S. B. Puttagunta, D. K. Sigalapalli, R. R. Bhandare, and A. B. Shaik. (2022). "An overview on applications of SwissADME web tool in the design and development of anticancer, antitubercular and antimicrobial agents: A medicinal chemist's perspective". *Journal of Molecular Structure.* **1259**. 10.1016/j.molstruc.2022.132712.

[23] P. H. Riyadi, Romadhon, I. D. Sari, R. A. Kurniasih, T. W. Agustini, F. Swastawati, V. E. Herawati, and W. A. Tanod. (2021). "SwissADME predictions of pharmacokinetics and drug-likeness properties of small molecules present in Spirulina platensis". *IOP Conference Series: Earth and Environmental Science.* **890** (1). 10.1088/1755-1315/890/1/012021.

[24] P. Banerjee, E. Kemmler, M. Dunkel, and R. Preissner. (2024). "ProTox 3.0: a webserver for the prediction of toxicity of chemicals". *Nucleic Acids Research.* **52** (W1): W513-W520. 10.1093/nar/gkae303.

[25] P. Banerjee, A. O. Eckert, A. K. Schrey, and R. Preissner. (2018). "ProTox-II: a webserver for the prediction of toxicity of chemicals". *Nucleic Acids Research.* **46** (W1): W257-W263. 10.1093/nar/gky318.

[26] E. Krieger and G. Vriend. (2015). "New ways to boost molecular dynamics simulations". *Journal of Computational*

Chemistry. **36** (13): 996-1007. 10.1002/jcc.23899.

[27] K. Imada, E. Sakai, H. Kato, T. Kawabata, S. Yoshinaga, T. Nehira, H. Terasawa, and S. Tsukamoto. (2013). "Reticulatins A and B and hyrtioreticulin F from the marine sponge Hyrtios reticulatus". *Tetrahedron.* **69** (34): 7051-7055. 10.1016/j.tet.2013.06.043.

[28] J. Yuvaniyama, P. Chitnumsub, S. Kamchonwongpaisan, J. Vanichtanankul, W. Sirawaraporn, P. Taylor, M. D. Walkinshaw, and Y. Yuthavong. (2003). "Insights into antifolate resistance from malarial DHFR-TS structures". *Nature Structural & Molecular Biology.* **10** (5): 357-65. 10.1038/nsb921.

[29] R. Ferreira de Freitas and M. Schapira. (2017). "A systematic analysis of atomic protein-ligand interactions in the PDB". *MedChemComm.* **8** (10): 1970-1981. 10.1039/c7md00381a.